Biogeosciences

Open Access

A newly observed physical cause of the onset of the subsurface spring phytoplankton bloom in the southwestern East Sea/Sea of Japan

Y.-T. Son[1], K.-I. Chang[1], S.-T. Yoon[1], T. Rho[2], J. H. Kwak[3], C. K. Kang[3], and K.-R. Kim[4]

[1]Research Institute of Oceanography/School of Earth and Environmental Sciences, Seoul National University, Seoul, 151-742, Korea
[2]Department of Oceanography/Marine Research Institute, Pusan National University, Busan 609-735, Korea
[3]POSTECH Ocean Science and Technology Institute, Pohang University of Science and Technology, Pohang, 790-784, Korea
[4]School of General Studies, GIST College, Gwangju Institute of Science and Technology, Gwangju, 500-712, Korea

Correspondence to: K.-I. Chang (kichang@snu.ac.kr)

Abstract. An ocean buoy, UBIM (Ulleung Basin Integrated Mooring), deployed during the spring transition from February to May 2010 reveals for the first time highly resolved temporal variation of biochemical properties of the upper layer of the Ulleung Basin in the southwestern East Sea/Sea of Japan. The time-series measurement captured the onset of subsurface spring bloom at 30 m, and collocated temperature and current data gives an insight into a mechanism that triggers the onset of the spring bloom not documented so far. Low-frequency modulation of the mixed layer depth ranging from 10 m to 53 m during the entire mooring period is mainly determined by shoaling and deepening of isothermal depths depending on the placement of UBIM on the cold or warm side of the frontal jet. The occurrence of the spring bloom at 30 m is concomitant with the appearance of colder East Sea Intermediate Water at buoy UBIM, which results in subsurface cooling and shoaling of isotherms to the shallower depth levels during the bloom period than those that occurred during the pre-bloom period. Isolines of temperature-based NO_3 are also shown to be uplifted during the bloom period. It is suggested that the springtime spreading of the East Sea Intermediate Water is one of the important factors that triggers the subsurface spring bloom below the mixed layer.

1 Introduction

The East Sea/Sea of Japan (East Sea hereafter) is a semi-enclosed deep marginal sea in the northwestern Pacific with mean water depth of about 1800 m (Fig. 1). It comprises three deep basins deeper than 2000 m: the Japan Basin in the northern half, the Ulleung Basin (UB) to the southwest, and the Yamato Basin to the southeast. The East Sea is horizontally divided by the warm water region to the south and the cold water region to the north with the subpolar front in between them, and the vertical water column consists of upper, intermediate, and deep layers. The upper layer corresponds to roughly upper 100 m above the main pycnocline, and contains the mixed layer and seasonal pycnocline. The Tsushima Warm Water (TWW) occupying the upper layer is carried by the Tsushima Current originating from the Kuroshio through Korea Strait. The Tsushima Current bifurcates into two main branches downstream of the Korea Strait. One of the branches, the East Korea Warm Current (EKWC), follows the east coast of Korea, separates from the coast at around 38° N, and meanders to the east. The meandering of the EKWC often accompanies the generation of mesoscale eddies (Chang et al., 2004). The intermediate and deep layers are all below the main pycnocline, or partly include the lower pycnocline. Water masses occupying the intermediate and deep layers south of the subpolar front are all formed in the Japan Basin (Kim et al., 2004; Talley et al., 2006).
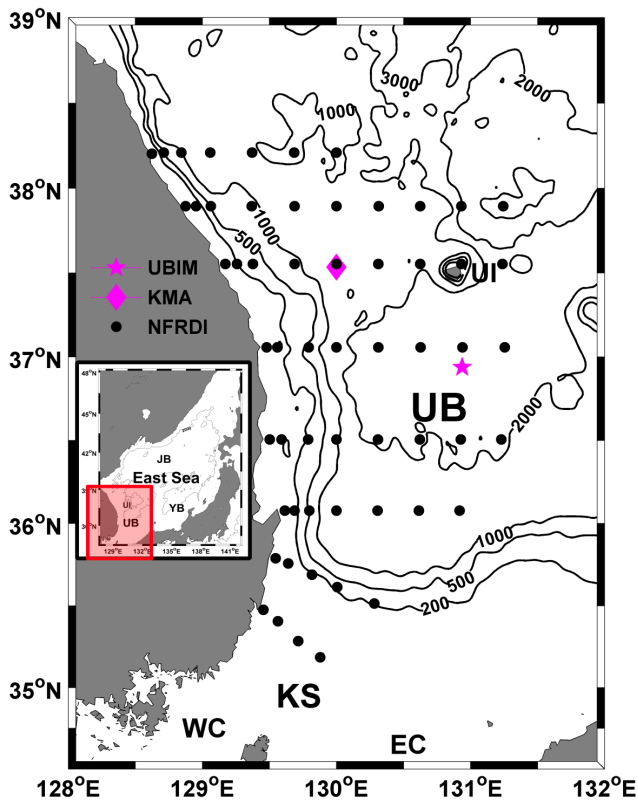
Fig. 1. Locations of buoy UBIM (star), meteorological buoy station (KMA, diamond) operated by the Korea Meteorological Agency, and bi-monthly serial oceanographic stations occupied by the National Fisheries Research and Development Institute (circles) in the Ulleung Basin of the southwestern East Sea. Contours are isobaths of 200, 500, 1000, 2000, and 3000 m. UB, JB, YB, KS, WC, EC, and UI denotes the Ulleung Basin, Japan Basin, Yamato Basin, Korea Strait, eastern and western channels of Korea Strait, and Ulleungdo Island, respectively.

The East Sea Intermediate Water (ESIW) characterized by a layer of shallow salinity minimum with a potential temperature range of 1–5 °C is widespread south of the subpolar front in a depth range of 100–500 m (Kim and Chung, 1984; Kim and Kim, 1999). The ESIW found offshore in the UB is brought into the basin through processes of subduction along the subpolar front (Lee et al., 2006). The ESIW is also carried by the North Korea Cold Current (NKCC) along the east coast of Korea (Cho and Kim, 1994). In spite of its prevalence south of the subpolar front, the influence of the ESIW and its circulation on marine ecosystem is largely unknown.

One of the important biological features of the East Sea is the bimodality of phytoplankton bloom at the sea surface with a strong spring bloom and weak fall bloom, which have been identified mainly from satellite ocean color data (Kim et al., 2000; Yamada et al., 2004, 2005). A compilation of the satellite data further revealed large interannual and decadal variation in the timing of spring bloom (Yamada et al., 2004; Yamada and Ishizaka, 2006). Attempts have been made to ex-

plain the initiation and development of spring bloom in the East Sea using the critical depth hypothesis (Kim et al., 2000; Yamada et al., 2004; Yamada and Ishizaka, 2006), where the mixed layer depth (MLD) is the crucial physical factor for the onset of spring bloom (Sverdrup, 1953). As the shoaling of the springtime MLD was thought mainly to result from the weakening of wind and vernal warming, wind speed variation is also regarded as an important factor for the interannual variations in the initiation timings for spring bloom (Yamada, 2005; Kim et al., 2007).

A subsurface chlorophyll maximum (SCM) layer has been frequently observed in vertical profiles of chlorophyll *a* concentration in a wide area of the UB (Shim and Park, 1996; Rho et al., 2012). The SCM layer is mainly observed between 30–40 m depth, and may last for six months in the UB from May to October (Rho et al., 2012). Previous studies suggest that the primary production at the SCM contributes significantly to the total annual primary production in the UB (Shim et al., 1992; Kwak et al., 2013). Development, duration, and temporal variability of the SCM, however, are poorly known.

Annual primary production in the UB is the highest in the East Sea: $222\,\mathrm{g\,C\,m^{-2}\,yr^{-1}}$ based on satellite ocean color data (Yamada et al., 2005). Monthly water column data yields the annual primary production of $273.0\,\mathrm{g\,C\,m^{-2}\,yr^{-1}}$ in the UB, about 20 % higher than the production inferred from the ocean color data, primarily due to the existence of the SCM layer (Kwak et al., 2013). The maintenance of the high primary production in the UB has been attributed to wind-induced coastal upwelling (Park and Kim, 2010), surface circulation (Yoo and Park, 2009), and mesoscale eddies (Hyun et al., 2009). As the TWW carried by the Tsushima Current is nutrient depleted, it is suggested that large volume transport through Korea Strait inhibits the onset of spring bloom (Yoo and Kim, 2004). This argument, however, is contrary to model results which suggest the nutrient supply from the Tsushima Current through Korea Strait (Kim et al., 2013) is the main source of primary production in the UB (Onitsuka et al., 2007). Hence, the role of the Tsushima Current in regulating the productivity south of subpolar front is still in contention.

Previous studies on the primary production and chlorophyll *a* distribution in the East Sea are based mostly on weekly or monthly composites of satellite ocean color data or sparse snapshots from survey results. Since the biological, as well as physical, processes are expected to be highly intermittent and have broad range of timescales from minutes to days and months, observations of biochemical parameters with coarse temporal resolution can cause aliasing, and episodic events cannot be adequately resolved.

This paper reports results from the first highly resolved time series of biochemical and collocated physical data in the UB obtained during the spring transition in 2010. Based on the temporal variation of chlorophyll measured at 30 m, our study highlights an important role of advection of subsurface water mass (ESIW) in triggering the subsurface spring

bloom below the surface mixed layer, which, so far to our knowledge, has not been documented.

2 Data and processing

Ocean buoy UBIM (Ulleung Basin Integrated Mooring), equipped with physical and biochemical sensors, was deployed in the middle of the UB at about 2160 m depth on 23 February and recovered on 30 May 2010 (Fig. 1). Due to damage of the mooring line, some sensors malfunctioned and data were not recorded. Available data from buoy UBIM include temperature from 10 m to 110 m at every 10 m interval, current profiles in the upper 100 m, chlorophyll fluorescence (CF) at 30 m, and PAR (photosynthetically active radiation) at 20 m from 23 February to 8 May.

Ancillary data sets are also used to interpret results from the single-point mooring: surface geostrophic currents based on satellite altimeter products distributed by AVISO and coastal sea level data (Choi et al., 2012), bimonthly serial CTD (conductivity–temperature–depth) data acquired in the UB by the National Fisheries Research and Development Institute (NFRDI) in February and April, 2010 (Fig. 1). During the period of buoy UBIM deployment, meteorological data of wind, surface pressure, and air temperature are acquired at the KMA (Korea Meteorological Agency) meteorological buoy station, which is located at about 100 km northwest of buoy UBIM (Fig. 1). Net heat flux and short-wave radiation data near buoy UBIM are archived from a $0.5° \times 0.5°$ gridded MERRA (Modern-Era Retrospective analysis for Research and Application) reanalysis product (http://disc.sci.gsfc.nasa.gov/daac-bin/DataHoldings.pl). Wind speed from MERRA product at the mooring location is well compared with that obtained at KMA station.

Observed time-series data exhibits multiple-scale temporal variability including a short-term variability less than diurnal period. Because this study intends to investigate the low-frequency variation of biochemical properties focusing on the onset of the spring bloom, time-series data are low-pass filtered with a cut-off frequency of 48 h to eliminate the short-term variability. Current data are corrected for magnetic variation, decomposed into east–west (u) and north–south (v) components, and are low-pass filtered. The same filter is also applied to other time-series data including meteorological data.

The fluorometer and PAR sensors were all calibrated by the factory prior to the deployment. The term CF (chlorophyll fluorescence) used in this paper is regarded as the factory-calibrated chlorophyll a concentration (μg L^{-1}) according to the manufacturer's (WET Lab) guidance. During the mooring period of buoy UBIM, in situ water samples were collected and the measured in situ chlorophyll concentration at 30 m determined by the spectrophotometry was 1.2 μg L^{-1}, similar to the CF value of 1.1 μg L^{-1} measured at the time of in situ water sampling. The second calibration of
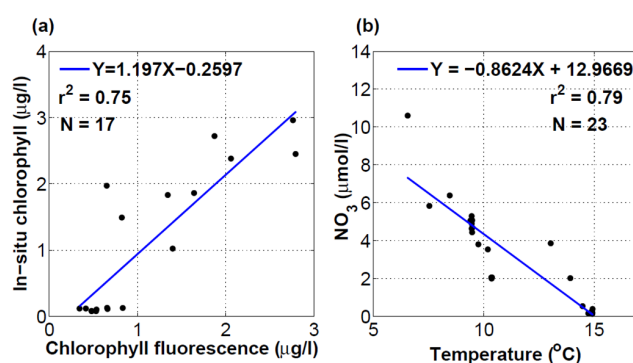
Fig. 2. (a) Cross-correlation (r^2) and linear regression between chlorophyll fluorescence (CF) measured by the fluorometer used in buoy UBIM and chlorophyll concentration determined from in situ water samples by spectrophotometry. The water samples were collected at a coastal site in the southwestern East Sea in July and October, 2011. **(b)** Cross-correlation (r^2) and linear regression between temperature and bottle NO$_3$ measurements. Temperature and NO$_3$ data were obtained in the Ulleung Basin in May, 2010 and March and April, 2011. Based on a linear regression shown in **(b)**, temperature-based NO3 concentration was estimated shown in Fig. 3d.

the fluorometer was made at a coastal site off the east coast of Korea in July and October 2011 by comparing CF values measured with the same fluorometer used in buoy UBIM and chlorophyll values of 17 in situ water samples taken every 3 h. Statistically significant correlation ($r^2 = 0.75$) was obtained between the CF values and in situ chlorophyll concentrations (Fig. 2a).

While nutrient data is important to understand observed temporal variation of CF, it is unavailable from the mooring. Reports have been given of the relationship between NO$_3$ and temperature in the East Sea in August based on long-term NFRDI data (Son et al., 2006), and also in other regions (Omand et al., 2012; Palacious et al., 2013). Nutrient and temperature data obtained in the UB on May in 2010 and on March and April in 2011 (Kwak et al., 2013) are used to test any possible temperature–NO$_3$ relationship in spring (Fig. 2b). NO$_3$ concentrations are inversely correlated with temperature with a significant correlation at 99 % confidence level ($r^2 = 0.79$). We also examined the temperature–NO$_3$ relationship using the method of Son et al. (2005) based on NFRDI data, which yields a similar good correlation. Temperature-based NO$_3$ is then estimated based on linear regression relationship with data obtained in 2010 and 2011 (Fig. 2b), and used to infer time series of NO$_3$ during the mooring period (Fig. 3d). The local relationship, however, should be used only for the spring (March–May) in the southwestern East Sea.
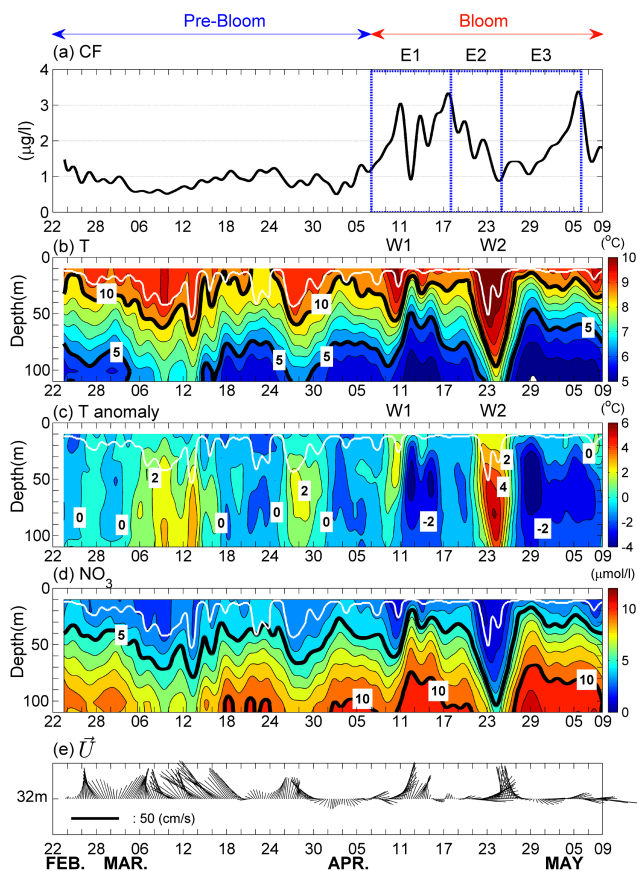
Fig. 3. Low-pass filtered time-series of **(a)** chlorophyll fluorescence at 30 m, **(b)** temperature, **(c)** temperature anomaly, **(d)** temperature-based NO$_3$, and **(e)** current at 32 m. Mixed layer depth is shown in white lines in **(b–d)**. E1, E2, and E3 in **(a)** indicate the three events during the bloom period. W1 and W2 in **(b)** and **(c)** denote two warm events occurred during the bloom period.

3   Results

3.1   Mean seawater and atmospheric properties during the pre-bloom and bloom periods

The CF variation is characterized by overall high values in the 2nd half of the mooring period from about 7 April (Fig. 3a). The period between 7 April and 8 May is referred to as the bloom period, and the pre-bloom period corresponds to the period before the bloom period from the beginning of the mooring. Table 1 summarizes biochemical, optical, and physical properties averaged over the pre-bloom and bloom periods. Mean CF values became doubled from 0.9 µg L^{-1} during the pre-bloom period to 1.9 µg L^{-1} during the bloom period. Although the mean solar radiation increased during the bloom period, mean PAR value at 20 m was about halved during the bloom period. While mean temperature at 20 m depth during the bloom period increased by 0.2 °C, mean temperature at 100 m during the bloom period was significantly lowered by 1.1 °C. In association with the subsurface

cooling, mean depth of 5 °C isotherm (upper boundary of the ESIW) was lifted from 87.8 m during the pre-bloom period to 71.0 m during the bloom period. Mean depth of 10 °C isotherm slightly shoaled from 36.6 m to 35.3 m between the pre-bloom and bloom periods. Mean currents and kinetic energy of low-frequency currents during the bloom period are weaker than those in the pre-bloom period. The mixed layer depth (MLD) is defined as the depth at which temperature is 0.2 °C cooler than temperature at 10 m assuming the water column shallower than 10 m is isothermal. Mean MLD was shoaled by about 8 m from the pre-bloom period (22.7 m) to the bloom periods (14.9 m). Hence, the time-series data at 30 m was mainly obtained below the surface mixed layer.

3.2   Temporal variations of physical properties

Over the mooring period, temperature in the upper 110 m ranged from 1 °C to 13 °C that corresponds to temperature ranges of the TWW ($T > 10$ °C), and the ESIW (1 °C $< T < 5$ °C). Low-frequency variability of the displacement of isotherms with a period of about 10–15 days is obvious, characterized by uplifting and lowering of isotherms (Fig. 3b). The uplifting of isotherms is accompanied by the appearance of a thick ESIW layer. Based on the 5 °C water at 110 m depth, the ESIW was captured five times during the entire mooring period with its duration of 9–14 days. Mean thickness of the ESIW, measured from 110 m upward to the depth of 5 °C isotherm, increased from about 28 m in the pre-bloom period to 65 m in the bloom period. Concomitant with the thickening of the ESIW, the minimum temperature of the ESIW at 110 m decreased from 3–4 °C in the pre-bloom period to 2–3 °C in the bloom period. When the ESIW disappeared, thick warm water layers with temperatures higher than 10 °C occupied the upper 60 m with an exceptionally thick warm water layer in late April extending down to 95 m together with maximum temperature greater than 13 °C.

The temperature anomaly map (Fig. 3c) clearly shows the alternating cold and warm anomalies that correspond to the periods of shoaling and deepening of isotherms, respectively. The temperature anomaly is calculated by subtracting low-pass filtered temperature from the record-length mean temperature at each depth. Four warm anomalies occurred during the entire mooring period, two in the pre-bloom period and another two in the bloom period (W1 and W2). Cold anomalies also occurred both in the pre-bloom and bloom periods, but with lower anomaly values (< -2 °C) during the bloom period, indicative of the subsurface cooling due to the uplifts of isotherms (Fig. 3b, Table 1). The MLD ranged from 11 m to 53 m during the entire mooring period. The low-frequency modulation of the MLD is characterized by the deepening and shoaling of the MLD in association with the lowering and uplifting of subsurface isotherms.

Northeastward or northwestward currents were predominantly observed at buoy UBIM during the mooring period (Fig. 3e). Record-length mean currents at 32 m at buoy

Table 1. Mean values of parameters for pre-bloom and bloom periods. Negative sign of net heat flux means net heating.

Parameters	Pre-bloom period	Bloom period
Wind speed ($m\,s^{-1}$)	6.7	5.8
Short-wave radiation ($W\,m^{-2}$)	169.6	224.0
Net heat flux ($W\,m^{-2}$)	57.9	−67.1
Chlorophyll fluorescence at 30 m ($\mu g\,L^{-1}$)	0.9	1.9
Dissolved oxygen at 30 m ($mL\,L^{-1}$)	6.3	6.5
PAR at 20 m ($\mu E\,m^{-2}\,s^{-1}$)	29	15
Mixed layer depth (m)	22.7	14.9
Temperature at 20 m (°C)	10.7	10.9
Temperature at 100 m (°C)	4.7	3.6
Depth of 10° isotherm (m)	36.6	35.3
Depth of 5° isotherm (m)	87.8	71.0
Current at 20 m ($cm\,s^{-1}$)	16.6	14.4
Current at 100 m ($cm\,s^{-1}$)	9.4	7.9
Kinetic energy of 20 m	316.0	268.0
Low-frequency currents ($cm^2\,s^{-2}$) 100 m	90.0	62.0

UBIM are directed to the north with a mean speed of about $10\,cm\,s^{-1}$. Low-frequency fluctuations, however, are notable with maximum speeds of about $50\,cm\,s^{-1}$ at 32 m. Temporal fluctuations of the currents are quasi-barotropic in the upper 100 m with reduced speeds below 60 m or 80 m. Strong currents with speeds greater than $30\,cm\,s^{-1}$ persisted relatively long from 26 February to 19 March with current fluctuations on timescales of about 3–4 days. After 20 March, relatively strong currents were then observed three times, 25–28 March, 9–13 April, and 21–27 April, thus persisting about 4–7 days. The periods of the occurrence of strong currents corresponded to those of the appearance of warm waters and the deepening of the MLD, indicating that the buoy UBIM was directly influenced by the strong horizontal currents. During these periods, the time-series data was acquired within or just below the MLD. When the isotherms were uplifted with the appearance of the thick ESIW, the upper currents became weak.

3.3 Temporal variation of chlorophyll fluorescence

While the low-frequency variation of temperature occurred during the entire mooring period, the CF variation at 30 m was weak and CF values remained below $1.5\,\mu g\,L^{-1}$ in the pre-bloom period (Fig. 3a). It is noted, however, that the variations between CF and temperature anomaly are related to each other, higher (lower) CF during cold (warm) anomaly even in the pre-bloom period. An initiation of subsurface bloom took place with the CF value sharply increasing to $3.0\,\mu g\,L^{-1}$ between 7 April and 11 April. The temporal variation of CF during the bloom period was characterized by large low-frequency fluctuations on timescales of about 7–20 days with peak-to-peak amplitudes ranging from $0.9\,\mu g\,L^{-1}$ to $3.3\,\mu g\,L^{-1}$. The bloom period corresponded to the period when the overall subsurface isotherms were uplifted

as compared to those during the pre-bloom period and, as a consequence, temperature of subsurface waters was lowered (Table 1). Temperature difference between pre-bloom and bloom periods at each depth level indicates the warming at 10 and 20 m and cooling at depth levels below with a maximum cooling of about 1.2 °C at 60–80 m (not shown).

Deepening and shoaling of isolines of temperature-based NO_3 occurred in conjunction with those of isotherms during the mooring period (Fig. 3d). In the bloom period, the NO_3 isolines were uplifted closer to the surface during the periods of two cold events as compared to the uplifts during the cold events in the pre-bloom period. The two warm events in the bloom period (W1 and W2 in Fig. 3c) were accompanied by low NO_3 concentrations, indicating that the TWW carried by the EKWC is nutrient-depleted water.

Two peak values of low-pass filtered CF greater than $3.0\,\mu g\,L^{-1}$ occurred on 17 April and 5 May (Fig. 3a). Considering the low-frequency variation of CF with its two peak values, we divide the bloom period into three events, from 7 April to 17 April (increasing CF), from 17 April to 24 April (decreasing CF), and from 25 April to 5 May (re-increasing CF) to examine the CF variation more in detail in conjunction with variations of physical parameters.

3.3.1 Event 1 (E1, 7 April to 17 April)

CF increased from 7 April to 11 April, and experienced a sharp drop between 11 April and 12 April (Fig. 3a). A high CF value ($> 2.0\,\mu g\,L^{-1}$) was recovered in a day on 13 April, and persisted until the end of event 1 with a peak value of $3.3\,\mu g\,L^{-1}$ on 17 April. Temperature time series in the upper 110 m during event 1 are characterized by the appearance of about 40 m thick warm water layer ($T > 12.0$ °C) between 9 and 11 April (W1 in Fig. 3b). The MLD becomes 26 m thick due to the occurrence of the warm water layer. The uplift of subsurface isotherms immediately followed and the warm layer was quickly shrunk. The 10 °C isotherm reached the shallowest depth less than 20 m on 11 April from 55 m on 9 April. Afterwards, isotherms of 9 °C and those less than 9 °C gradually deepened while fluctuating vertically with a period of about 3–4 days. The 10 °C isotherm also experienced the vertical fluctuations, but it showed no distinct deepening until the end of event 1. Associated with the uplift of subsurface isotherms, the MLD shoaled to be less than 15 m during the 2nd half of event 1.

The appearance of the warm water at the beginning of event 1 (W1) was concomitant with an initiation of strong eastward currents. Strong northward currents then followed, hence the currents turned cyclonically, while the isotherms experienced the shoaling. The low-frequency currents remained weak during the rest of the period of event 1 when subsurface isotherms and NO_3 isolines were uplifted and CF remained high with a peak value on 17 April.

3.3.2 Event 2 (E2, 18–24 April)

After the 1st peak on 17 April, CF decreased gradually until 24 April (Fig. 3a). Temperature fluctuations during event 2 is characterized by the re-emergence of the warm water layer with temperature higher than 12 °C (W2) similar to that during the 1st half of event 1, but now with longer duration, deep-reaching structure, and highest warm anomaly (Fig. 3b, d). The warm water ($T > 12.0$ °C) first appeared on 20 April and was observed until 25 April at 10 m. The warm water layer thickened, and the maximum thickness of the warm layer reached 75 m on 23 April. MLD deepened from about 12 m on 21 April to 51 m on 23 April, and then shoaled again less than 20 m on 25 April.

Strong eastward currents were observed from 21 April when the warm water layer started to deepen, which persisted until 23 April and then strong northward currents followed (Fig. 3e). The appearance of the warm water layer concomitant with strong eastward currents followed by strong northward currents is similar to those that occurred in W1 period; the CF variation, however, is different. CF increased in W1 period, while it decreased in W2 period. Both W1 and W2 periods corresponded to the direct influence of the EKWC to buoy UBIM, and this different CF response indicates the different role of the warm surface current in chlorophyll variation, which will be discussed shortly.

3.3.3 Event 3 (E3, 25 April–5 May)

After a local minimum of CF less than $0.9\,\mu\text{g}\,\text{L}^{-1}$ on 24 April, CF slightly increased to $1.4\,\mu\text{g}\,\text{L}^{-1}$ on 26 April and then decreased again to $1.0\,\mu\text{g}\,\text{L}^{-1}$ on 28 April (Fig. 3a). Then CF increased almost monotonically from 28 April to 5 May to reach the 2nd CF peak ($> 3.0\,\mu\text{g}\,\text{L}^{-1}$). A sharp CF decrease was then followed after 5 May.

4 Discussions

The time-series observation at buoy UBIM captured a biological transition from the pre-bloom to bloom periods. According to mean properties during those two periods, the transition was concurrent with the weakening of wind intensity, net oceanic heat gain, shoaling of the MLD, and subsurface cooling in conjunction with the uplifting of subsurface isotherms. The former three features would support the Sverdrup hypothesis and have been documented to explain the observed spring bloom at the surface (above the mixed layer) based on satellite ocean color data. The time-series data, however, was acquired mostly below the surface mixed layer, and the focus of this study is on the onset of the bloom below the mixed layer due to the subsurface cooling. The present observation highlights three distinct features. First, the CF variation is closely related with the deepening and shoaling of isotherms during the mooring period in such a way that the shoaling of isotherms are concurrent with the increases in CF. The
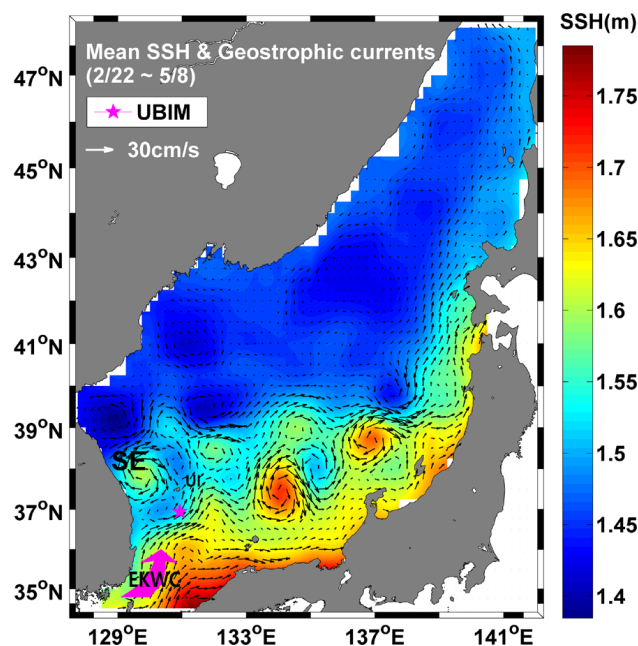
Fig. 4. Mean surface geostrophic currents and sea surface height in the East Sea during the deployment of buoy UBIM (star) calculated from AVISO satellite altimeter data combined with coastal sea level data (Choi et al., 2012). EKWC and SE denote the East Korean Warm Current and the Sokcho Eddy, respectively.

linkage is recognized during both the pre-bloom and bloom periods, but more pronounced during the bloom period leading to the spring bloom at 30 m. Second, the bloom period at 30 m corresponds to the uplifted subsurface isotherms and NO$_3$ isolines on average as compared to those in the pre-bloom period. Lastly, the deepening of isotherms associated with the warm water advection occurred twice (W1 and W2 in Fig. 3c) during the bloom period but their effects on the CF variation were different. In this section, we interpret the features using ancillary data sets.

4.1 Upper circulation during the mooring period

According to mean surface circulation during the deployment of buoy UBIM, the EKWC, after entering through Korea Strait, flows northward hugging the east coast of Korea south of 37° N, separates from the coast to flow eastward, and turns northward at around 131° E after merging with a part of the northward flow coming from the eastern channel of Korea Strait (Fig. 4). The separated EKWC then flows northeastward as a meandering jet, and the meander amplitude appears to be amplified downstream. An anticyclonic eddy with diameter greater than 100 km and maximum surface velocity of about $30\,\text{cm}\,\text{s}^{-1}$ can be seen off the east coast of Korea, the Sokcho Eddy (Kim et al., 1999). The buoy UBIM was located on the cyclonic side of the meandering EKWC. During the entire mooring period, the surface circulation is generally similar to the mean current pattern shown in Fig. 4, but with
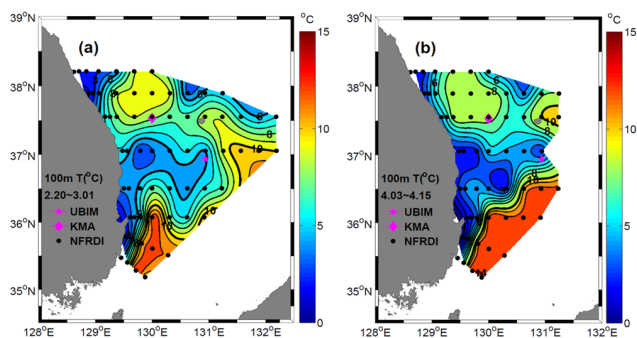
Fig. 5. Temperature distributions at 100 m in the Ulleung Basin in **(a)** February and **(b)** April, based on NFRDI bi-monthly data acquired in 2010.

Fig. 6. (a) Temperature difference at 100 m between February and April, 2010. **(b)** Temperature anomaly at 100 m in April, 2010 with respect to the long-term mean April temperature at 100 m between 1976 and 2010. In the temperature difference map, the negative sign represents the lowering of temperature in April as compared to that in February. In the anomaly map, the negative sign indicates the cold anomaly in April, 2010 as compared to the climatological mean. White lines on both maps denote 0 values.

a short-term path variability of the EKWC that is reflected in the observed upper currents (Fig. 3e; also see Fig. 8).

The north and northeastward path of the EKWC in Fig. 4 would mainly follow the thermal front at 100 m (Ichiye and Takano, 1988) with deep thermocline and warm waters on the anticyclonic side of the front. The inferred circulation from the temperature distribution at 100 m in February and April 2010 (Fig. 5) is similar to the geostrophic circulation in Fig. 4. In April, the path of the EKWC shifted to the northwestward, and the warm region with temperature higher than 10 °C had been expanded south of 37° N. The anticyclonic Sokcho Eddy shown in Fig. 4 was also identified in the temperature maps with isolated warm waters west of 130.5° E and north of 37° N. Anticyclonic eddies found in the UB is characterized by a thick warm subsurface layer topped by surface water colder than surrounding warm filament in stratified seasons (Chang et al., 2004).

4.2 Interpretation of temperature fluctuations at buoy UBIM

The horizontal current and temperature maps (Figs. 4, 5) indicate that the shoaling and deepening of isotherms (and alternating warm and cold anomalies in Fig. 3c) observed during the mooring period at buoy UBIM resulted from the variability of thermal front. When the frontal boundary moved from the region northwest of the buoy to the southeast, the placement of the buoy also shifted from the warm (anticyclonic) side of the front to cold (cyclonic) side of the front, and then subsurface isotherms became shallow from deeper depths. The observed strong currents at buoy UBIM corresponded to the periods when the buoy was located near the front and influenced directly by the EKWC after its separation from the coast. The low-frequency frontal variability is thought to be associated with the path variability of the EKWC, although it is uncertain what caused the variability.

4.3 Effect of the ESIW advection on the spring bloom

The low-frequency fluctuations of temperature described in the above are related to those of CF, in that the CF values increase when the isotherms shoal and vice versa. Although this relationship can be found both in the pre-bloom and bloom periods, the large fluctuations of CF with peak CF values exceeding $3.0\,\mu g\,L^{-1}$ occurred only during the bloom period. Furthermore, this bloom period corresponds to the period of uplifted isotherms (and NO_3 isolines) and subsurface cooling on average as compared to those in the pre-bloom period (Table 1).

According to basin-wide temperature change between February and April, cooling at 100 m from February to April was widespread in the UB except two regions affected by the Sokcho Eddy in the northwestern basin and by the separated EKWC in the southern and southeastern periphery of the basin (Fig. 6a). We also examined climatological basin-averaged temperature variation at 100 m and 200 m in the UB using the NFRDI taken between 1976 and 2010 (Fig. 7). The mean temperatures at 100 m and 200 m also show the temperature decrease from February and April, suggesting that the subsurface cooling observed in April 2010 was not anomalous but represents the mean feature. Annual minimum temperature at both 100 m and 200 m occurs in August as was also noted by previous works (Shin et al., 2013).

Both the moored observation at buoy UBIM and the climatological seasonal variation of subsurface temperature indicate that the springtime southward spreading of the ESIW to the UB resulted in lowering subsurface temperature and uplifting isotherms (and also NO_3 isolines) (Fig. 3b, c, d). Then the biological response to these changes contributes to the observed subsurface spring bloom below the MLD due to the availability of nutrients in the deep layer.
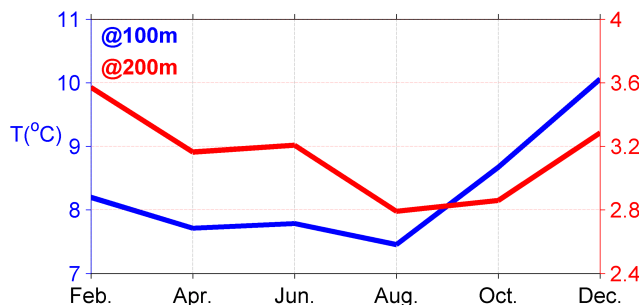
Fig. 7. Spatially averaged bi-monthly mean temperatures at 100 m and 200 m in the Ulleung Basin based on NFRDI data taken between 1976 and 2010.

Fig. 8. A 8-day composite images of MODIS chlorophyll *a* (color) during the periods of two warm events (W1 and W2 in Fig. 3b, c). Composite days in month and dates are shown in each figure. A 7-day composite SSH distributions close to the dates of the chlorophyll *a* maps are also shown with contour lines.

The uplifts of isotherms occurred twice (E1 and E3 in Fig. 3a) during the bloom period after the two warm episodes of W1 and W2. There was a short-term variation of CF during E1 period, which was described in the above. The peak CF values for both E1 and E3 occurred several days (6 days for E1 and 7 days for E3) after the subsurface isotherms and NO3 isolines were uplifted and reached to the shallowest depth levels. The time lag appears to be the timescale for the growth of phytoplankton.

We note that temperature at 100 m in April 2010 (also in February 2010, not shown) was anomalously low in the central part of the UB as compared to the climatological mean temperature (Fig. 6b). The appearance of the anomalously cold waters in 2010 could be due to the offshore shift of the EKWC path or the spreading of anomalously cold ESIW in winter and spring 2010 or both. During the winter of 2009/2010, unusually low temperatures were recorded over much of northern Eurasia and North America that were closely associated with the strongly negative phase of the Arctic Oscillation since 1950 (Wang et al., 2010). During the severe winter, surface waters north of the subpolar front would be cooled below average, and then the colder ESIW spreading to the south would contribute to the observed cold anomaly in the UB in February and April 2010. We have not looked into the reason for this anomalously low temperature of the ESIW in April 2010 exhaustively because it is beyond the scope of this study.

Modeling investigation of seasonal variation of the volume transport of the NKCC transporting the ESIW to the UB shows an increase in the transport from winter to spring with a secondary maximum transport in March (Kim et al., 2009). The seasonal variation of the ESIW in the UB based on salinity data also shows the bimodal low salinity peaks due to the ESIW in winter (January–March) and summer (July–September) (Shin et al., 2013). It is not clear whether the subsurface temperature also shows a secondary minimum in March, because NFRDI data is only available at even months. The temperature time series observed at buoy UBIM indicates the lower subsurface temperature in April than that in March at least in the central part of the UB in 2010. It should
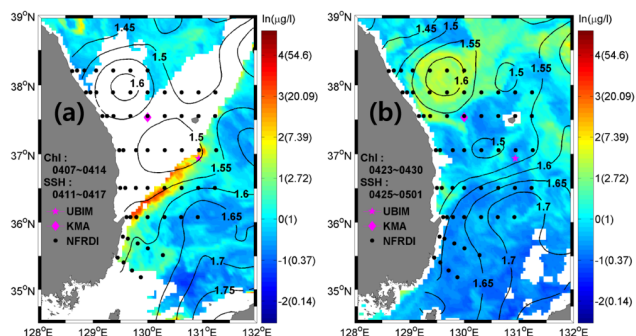
be noted that the physical properties of the ESIW also show a considerable interannual variation (Kim et al., 1991).

4.4 Effect of the EKWC advection on the chlorophyll variation

Deep-reaching warm waters with concurrent strong currents appeared twice during the bloom period, W1 (9–11 April) and W2 (21–26 April) (Fig. 3b, c). The CF variations during W1 and W2 periods, however, were different. A sharp increase in CF was accompanied by the appearance of warm water in W1 period, while a gradual decrease in CF occurred in W2 period.

Figure 8 shows the distribution of 8-day composite MODIS chlorophyll *a* distribution and 7-day composite sea surface height (SSH) during the periods of W1 and W2. Surface chlorophyll distribution in W1 period shows a high chlorophyll band extending from the southeast coast of Korea to the northeast following approximately the 1.55 m SSH isoline along the boundary of the separated EKWC (Fig. 8a). The separated EKWC carrying high surface chlorophyll from the coast swept over buoy UBIM. Currents at 32 m were strong in W1 period due to the direct influence of the EKWC (Fig. 3e). The MLD at buoy UBIM was 26 m in W1 period (Fig. 3b), and the observed initial increase in CF at 30 m at buoy UBIM between 7 and 11 April is thought to be due to this advection of high surface chlorophyll originating from the coast. The reason for the appearance of high chlorophyll in the coastal region is beyond the scope of this study, but may be due to coastal upwelling (Yoo and Park, 2009).

In W2 period, surface chlorophyll in the coastal region west of 130.5° E and south of 37.5° N was low, and high surface chlorophyll band along the outer edge of the separated EKWC observed in W1 period cannot be seen (Fig. 8b). The comparison of the surface chlorophyll distributions between W1 and W2 periods supports the previous works on the importance of the coastal source of high chlorophyll and the

role of horizontal advection either by large- or mesoscale circulation in making the UB the most productive region in the East Sea (Hyun et al., 2009; Yoo and Park, 2009). Without the coastal source, the EKWC carries nutrient-depleted water mass, and this explains the different effects of the EKWC advection observed at buoy UBIM during the periods of the two warm episodes.

4.5 Other possible factors affecting the CF variation

As buoy UBIM was located near the meandering frontal jet during the mooring period, where simultaneous upwelling and downwelling zones occur (Lima et al., 2002), vertical advection could also play a role in transporting nutrients upward, hence could contribute to the observed bloom at 30 m. Vertical velocity in the upper ocean is associated with the wind-induced Ekman pumping, meso- (e.g., McGillicuddy et al., 1998) and submesoscale features (e.g., Mahadevan and Tandon, 2006), and unstable fronts (e.g., Martin and Richards, 2001).

The observed cooling of the subsurface water in the bloom period as compared to that in the pre-bloom period could arise from the local Ekman pumping. Mean wind stress curl is calculated suing the MERRA product during the pre-bloom and bloom periods. It differs by about $0.1 \times 10^{-6} \, \mathrm{N \, m^{-2}}$ in the central UB, then the associated change in the Ekman pumping is about $3.6 \, \mathrm{m \, month^{-1}}$ which cannot account for the observed shoaling of $5 \,^{\circ}\mathrm{C}$ isotherm depth by 16.8 m in Table 1.

We interpreted the low-frequency fluctuations of the depth of isotherms observed at buoy UBIM as resulting from the movement of the thermal front along the path of the EKWC. The observed strengthening and weakening of horizontal currents at buoy UBIM during the transitional periods of the lateral displacement of the fronts supports this interpretation. The low-frequency fluctuations of isothermal depths, however, could be also due to vertical advection. Neglecting diffusion terms, horizontal and vertical velocities are roughly estimated from the temperature equation assuming horizontal and vertical advection are solely responsible for the observed local temperature change: $\partial T / \partial t + u_n \partial T / \partial n = 0$, $\partial T / \partial t + w \partial T / \partial z = 0$, where u_n and $\partial T / \partial n$ denote the cross-frontal velocity and temperature gradient, respectively. The cross-frontal temperature gradient was calculated using the horizontal temperature map in Fig. 5b, which was based on NFRDI data acquired between 3 and 15 April. The local temperature change and vertical gradient of temperature are calculated using data from buoy UBIM between 12 and 13 April. The calculation yields an order of magnitudes of about $30 \, \mathrm{cm \, s^{-1}}$ for horizontal velocity and $1.2 \times 10^{-2} \, \mathrm{cm \, s^{-1}}$ for vertical velocity. The estimated horizontal velocity scale is comparable to the observed velocity. The vertical velocity scale is also comparable to that occurs at the frontal region (Velez-Belchi and Tintore, 2001; Thomas et al., 2010), suggesting that the vertical advection could have also con-

tributed to the observed fluctuations of isothermal depths at buoy UBIM.

4.6 Implications

The continuous time-series measurement reveals the low-frequency variability of biochemical parameters as well as physical properties. The low-pass filtered CF values fluctuate from $0.9 \, \mu\mathrm{g \, L^{-1}}$ to $3.3 \, \mu\mathrm{g \, L^{-1}}$ during the bloom period, and the range becomes even higher for the unfiltered data. The low-frequency CF fluctuations have timescales of about 3–15 days and they are strongly linked to the circulation. The present observation strongly indicates that any sampling of biogeochemical properties with poor temporal resolution could seriously mislead the whole features.

Warming and a decrease in the dissolved oxygen contents of deep waters have been one of main issues on regional climate changes in the East Sea (e.g., Kim et al., 2004), which is attributed to changes in the ventilation system of the East Sea (Kang et al., 2004). The cessation of deep water formation was replaced with the sinking of surface waters to shallower depth levels (Postlewaite et al., 2005; Jenkins, 2008). The present study suggests the springtime advection of the ESIW influences the subsurface spring bloom in the UB together with other factors previously suggested. As the ESIW is a part of the East Sea's ventilation system, the implication of the present study is that the structural change in the subsurface water mass formation due to climate change would also result in changes in the ecosystem. This hypothesis needs to be extensively tested through field observations and model studies to understand the role of the ESIW and associated changes in subsurface waters and circulation in marine ecosystem of the East Sea.

4.7 Limitations of the present work

Limitations of the present study are recognized, using the scarcity of biological data on phytoplankton species, zooplankton grazing, and vertical structure of chlorophyll layer together with poorly resolved spatial distribution of physical parameters at the frontal region. According to Kwak et al. (2013), diatoms are generally the most dominant phytoplankton throughout the year in the UB, and especially, the subsurface chlorophyll maximum layer was found at 20–30 m, and it corresponded to the depth of maximum contribution of diatoms (> 90 %) in spring and summer 2010. Hence, any increase in the CF is thought to be mainly due to the spring bloom rather than due to any changes in the phytoplankton species.

Further interdisciplinary observations integrating moored measurements with spatial sampling in the use of shipboard profiling and remote sensing observations are necessary to understand the spring bloom in the East Sea. An extensive physical-biological coupled modeling will be also useful to better understand the interactions between the onset of the

spring bloom and the frontal jet together with biological factors in this highly productive UB of the East Sea.

5   Summary

Time-series measurement of biochemical, optical, and physical parameters near the frontal region in the southwestern East Sea between February and May in 2010 captured, for the first time, the onset of subsurface spring phytoplankton bloom. Mean chlorophyll concentration (CF) during the bloom period is twice higher than that during the pre-bloom period. Simultaneously obtained temperature and temperature-based NO_3 data show the uplifts and depressions of isotherms and NO_3 isolines concurrent with higher and lower CF, respectively. The fluctuations of isotherms at buoy UBIM arise from the placement of the mooring location between the cold side (shallow thermocline) and warm side (deep thermocline) of the front due to the short-term frontal variability set by the northeastward flowing EKWC.

The springtime advection of the ESIW originating from the northern East Sea towards the cold side of the front cooled subsurface waters, and shoaled subsurface isotherms (and MLD) and NO_3 isolines during the bloom period. Hence, the advection of the ESIW played a major role in triggering the observed subsurface spring bloom in the central UB at least during our mooring period. The moored observation together with ancillary data also clarified the different role of the EKWC advection in subsurface CF variation in the middle of the UB. When it carries the high-chlorophyll coastal water, the subsurface CF increased. Otherwise, the nutrient-depleted EKWC acts to lower the CF.

References

Chang, K.-I., Teague, W. J., Lyu, S. J., Perkins, H. T., Lee, D.-K., Watts, D. R., Kim, Y.-B., Mitchell, D. A., Lee, C. M., and Kim, K.: Circulation and currents in the southwestern East/Japan Sea: overview and review, Prog. Oceanogr., 61, 105–156, 2004.

Cho, Y.-K. and Kim, K.: Two modes of salinity-minimum layer water in the Ulleung Basin, La Mer, 32, 271–278, 1994.

Choi, B.-J., Byun, D.-S., and Lee, K.-H.: Satellite-altimeter-derived East Sea surface currents: Estimation, description and variability pattern, The Sea, J. Korean Soc. Oceanogr., 17, 225–242, 2012. (In Korean with English abstract)

Hyun, J. H., Kim, D., Shin, C.-W., Noh, J.-H., Yang, E.-J., Mok, J.-S., Kim, S.-H., Kim, H.-C., and Yoo, S.: Enhanced phytoplankton and bacterioplankton production coupled to coastal upwelling and an anticyclonic eddy in the Ulleung Basin, East Sea, Aquat. Microb. Ecol., 54, 45–54, 2009.

Ichiye, T. and Takano, K.: Mesoscale eddies in the Japan Sea, La Mer, 26, 69–79, 1988.

Jenkins, W. J.: The biogeochemical consequences of changing ventilation in the Japan/East Sea, Mar. Chem., 108, 137–147, 2008.

Kang, J. H., Kim, W.-S., Chang, K.-I., and Noh, J.-H.: Distribution of plankton related to the mesoscale physical structure within the surface mixed layer in the southwestern East Sea, Korea, J. Plankton Res., 26, 1515–1528, 2004.

Kim, C.-H., Lie, H.-J., and Chu, K.-S.: On the intermediate water in the southwestern East Sea (Sea of Japan), In: Ocean Hydrodynamics of the Japan and East China Seas, edited by Ichiye T., 55–65, Elsevier, Amsterdam, 1991.

Kim, H., Yoo, S., and Oh, I. S.: Relationship between phytoplankton bloom and wind stress in the sub-polar frontal area of the Japan/East Sea, J. Mar. Syst., 16, 205–216, 2007.

Kim, K. and Chung, J.-Y.: On the salinity-minimum layer and dissolved oxygen-maximum layer in the East Sea (Sea of Japan), In: Oceanography of Asian Marginal Seas, edited by Takano, K., Elsevier, Amsterdam, 129-141, 1984.

Kim, K., Kim, K.-R., Kim, Y.-G., Cho, Y.-K., Kang, D.-J., Takematsu, M., and Volkov, Y.: Water mass and decadal variability in the East Sea (Sea of Japan), Prog. Oceanogr., 61, 157–174, 2004.

Kim, S.-K., Chang, K.-I., Kim, B., and Cho, Y.-K.: Contribution of currents to the N abundance in the Northwestern Pacific marginal seas, Geophys. Res. Lett., 40, 143–148, 2013.

Kim, S. W., Saitoh, S. I., Ishizaka, J., Isoda, Y., and Kishino, M.: Temporal and spatial variability of phytoplankton pigment concentrations in the Japan Sea derived from CZCS images, J. Oceanogr., 56, 527–538, 2000.

Kim, S. Y., Lee, H. S., Min, D., and Yoon, H.-J.: Comparison of nonlinear 1 1/2-layer and 2 1/2-layer numerical models with strong offshore winds and the Tsushima Current in the East Sea, Environ. Sci., 3, 91–103, 1999.

Kim, Y.-G. and Kim, K.: Intermediate waters in the East/Japan Sea, J. Oceanogr., 55, 123–132, 1999.

Kim, Y. H., Chang, K.-I., Park, J. J., Park, S. K., Lee, S.-H., Kim, Y.-G., Jung, K. T., and Kim, K.: Comparison between a reanalyzed product by 3-dimensional variational assimilation technique and observations in the Ulleung Basin of the East/Japan Sea, J. Mar. Syst., 78, 249–264, 2009.

Kwak, J. H., Lee, S. H., Park, H. J., Choy, E. J., Jeong, H. D., Kim, K. R., and Kang, C. K.: Monthly measured primary and new productivities in the Ulleung Basin as a biological "hot spot" in the East/Japan Sea, Biogeosciences, 10, 4405–4417, doi:10.5194/bg-10-4405-2013, 2013.

Lee, C. M., Thomas, L. N., and Yoshikawa, Y.: Intermediate water formation at the Japan/East Sea subpolar front, Oceanography, 19, 110–121, 2006.

Lima, I. D., Olson, D. B., and Doney, S. C.: Biological response to frontal dynamics and mesoscale variability in oligotrophic environments: Biological production and community structure, J. Geophys. Res., 107, doi:10.1029/2000JC000393, 2002.

Mahadevan, A. and Tandon, A.: An analysis of mechanism for sub-mesoscale vertical motion at ocean fronts, Ocean Modell., 14, 241–256, 2006.

Martin, A. P and Richards, K. J.: Mechanisms for vertical nutrient transport within a North Atlantic mesoscale eddy, Deep-Sea Res. Pt. II, 48, 757–773, 2001.

McGillicuddy, D. J., Robinson, A. R., Siegel, D. A., Jannasch, H. W., Johnson, R., Dickey, T. D., McNeil, J., Michaels A. F., and Knap, A. H.: Influence of mesoscale eddies on new production in the Sargasso Sea, Nature, 394, 263–266, 1998.

Omand, M. M., Feddersen, F., Guza, R. T., and Franks, P. J. S.: Episodic vertical nutrient fluxes and nearshore phytoplankton blooms in Southern California, Limnol. Oceanogr., 57, 1673–1688, 2012.

Onitsuka, G., Yanagi, T., and Yoon, J.-H.: A numerical study on nutrient sources in the surface layer of the Japan Sea using a coupled physical-ecosystem model, J. Geophys. Res., 112, C05042, doi:10.1029/2006JC003981, 2007.

Palacios, D. M., Hazen, E. L., Schroeder, I. D., and Bograd, S. J.: Modeling the temperature-nitrate relationship in the coastal upwelling domain of the California Current, J. Geophys. Res., 118, 1–17, doi:10.1002/jgrc.20216, 2013.

Park, K.-A. and Kim, K.-R.: Unprecedented coastal upwelling in the East/Japan Sea and linkage to long-term large-scale variation, Geophys. Res. Lett., 37, L09603, doi:10.1029/2009GL042231, 2010.

Postlewaite, C. F., Rohling, E. J., Jenkins, W. J., and Walker, C. F.: A tracer study of ventilation in the Japan/East Sea, Deep-Sea Res. Pt. II, 52, 1684–1704, 2005.

Rho, T., Lee T., Kim, G., Chang, K.-I., Na, T., and Kim, K.-R.: Prevailing subsurface chlorophyll maximum (SCM) layer in the East Sea and its relation to the physic-chemical properties of water masses, Ocean Polar Res., 34, 412–430, 2012. (In Korean with English abstract)

Shim, J. H. and Park, J. K.: Primary production system in the southern waters of the East Sea, Korea III, Vertical distribution of the phytoplankton in relation to chlorophyll maximum layer, J. Korean Soc. Oceanogr., 31, 196–206, 1996.

Shim, J. H., Yeo, H. G., and Park, J. K.: Primary production system in the southern waters of the East Sea, Korea I. Biomass and productivity, J. Korean Soc. Oceanogr., 27, 91–100, 1992.

Shin, C.-W., Byun, S.-K., Kim, C., Lee, J.H., Kim, B.-C., Hwang, S.-C., Seung, Y. H., and Shin, H.-R.: Seasonal variations in the low-salinity intermediate water in the region south of sub-polar front of the East Sea (Sea of Japan), Ocean Sci. J., 48, 35–47, 2013.

Son, S., Platt, T., Bouman, H., Lee, D., and Sathyendranath, S.: Satellite observation of chlorophyll and nutrients increase induced by Typhoon Megi in the Japan/East Sea, Geophys. Res. Lett., 33, L05607, doi:10.1029/2005GL025065, 2006.

Sverdrup, H. U.: On condition for the vernal blooming of phytoplankton, Journal du Conseil International pour l'Exploration de la Mer, 18, 287–295, 1953.

Talley, L. D., Min, D.-H., Lobanov, V. B., Luchin, V. A., Ponomarev, V. I., Salyuk, A. N., Shcherbina, A. Y., Tishchenko, P. Y., and Zhabin, I.: Japan/East Sea water masses and their relation to the sea's circulation, Oceanography, 19, 32–49, 2006.

Thomas, L. N., Lee, C. M., and Yoshikawa, Y.: The subpolar front of the Japan/East Sea. Part II: Inverse method for determining the frontal vertical circulation, J. Phys. Oceanogr., 40, 3–25, 2010.

Velez-Belchi P. and Tintore J.: Vertical velocities at an ocean front, Scientia Marina, 65, 291–300, 2001.

Wang, C., Liu, H., and Lee, S.-K.: The record-breaking cold temperatures during the winter of 2009/2010 in the Northern Hemisphere, Atmos. Sci. Lett., 11, 161–168, 2010.

Yamada, K., Ishizaka, J., Yoo, S., Kim, H. C., and Chiba, S.: Seasonal and interannual variability of sea surface chlorophyll a concentration in the Japan/East Sea (JES), Prog. Oceanogr., 61, 193–211, 2004.

Yamada, K., Ishizaka, J., and Nagata, H.: Spatial and temporal variability of satellite estimated primary production in the Japan Sea from 1998 to 2002, J. Oceanogr., 61, 857–869, 2005.

Yamada, K. and Ishizaka, J.: Estimation of interdecadal change of spring bloom timing in the case of the Japan Sea, Geophys. Res. Lett., 33, L02608, doi:10.1029/2005GL024792, 2006.

Yoo, S. and Kim, H. C.: Suppression and enhancement of the spring bloom in the southwestern East Sea/Japan Sea, Deep-Sea Res. Pt. II, 51, 1093–1111, 2004.

Yoo, S. and Park, J.: Why is the southwest the most productive region of the East Sea/Sea of Japan, J. Mar. Syst., 78, 301–315, 2009.